Bubble entrapment by drop impact: Combined effect of surface tension and viscosity

Vincent Gourmandie, Juliette Pierre, Valentin Leroy, Caroline Derec

Bubble entrapment by drop impact: combined effect of surface tension and viscosity

Vincent Gourmandie,* Juliette Pierre,† Valentin Leroy,* and Caroline Derec‡

(Dated: October 4, 2024)

In this study, we systematically investigate the effect of surface tension on bubble entrapment after drop impact in the pinching regime. Experiments are conducted using three different systems: pure water, aqueous solutions with ethanol or with surfactant molecules, both at various concentrations. Results are compiled for a large set of values of the surface tension γ and the drop impact velocity U. Across all solutions, the cavity development dynamics exhibit similarity and are effectively characterized by dimensionless gravito-capillary parameters. Whatever the surface tension, our measurements indicate that only 40% of the impact energy is converted into potential energy of the cavity. However, a notable distinction arises when considering bubble entrapment. We have constructed a *bubbling diagram* in the (U, γ) plane, and observed that the conditions for bubble entrapment are altered with changing surface tension in water-ethanol mixtures. More intriguingly, these conditions are modified in a distinctly different manner for surfactant solutions. To interpret our experimental findings, we compile a comprehensive set of experimental and numerical results from the literature. We demonstrate the possibility of unifying results across all systems and our water-ethanol mixtures through an empirical law including the influence of surface tension and viscosity. Although no physical justification exists at this stage, this empirical law suggests the significant role of capillary waves traveling along the cavity interface in bubble entrapment. Within this context, the behavior of surfactant-laden solutions aligns with other homogeneous solutions by considering the elastic properties conferred upon the interfaces by surfactant molecules.

Drop impact, Bubble entrapment, Surface tension, viscosity, capillary waves

I. INTRODUCTION

The impact of droplets on a liquid bath has been studied for over a century [1, 2], first with the development of photography, and more recently with the rise of fast imaging techniques. The study of drop impact on deep liquid pool is a highly significant subject from a fundamental perspective, given the numerous associated phenomena. These include the analysis of the velocity field during the cavity development, the collapse of the cavity resulting in the generation of a jet (so-called Worthington jet), which breaks down into droplets. Under specific conditions of drop size and impact velocity, there is also the pinching of a bubble at the cavity's bottom. Such mechanisms play a role in various scenarios, such as the development of Rayleigh-Taylor instability during cavity development and the mixing of liquid drop and pool [3]. In addition, these mechanisms are involved in ocean-atmosphere exchange through droplet ejection [4, 5], as well as in the underwater sound produced by rain, capable of interfering with sonar systems [6]. This last situation is produced by the tiny bubble pinched at the bottom of cavity and is what we are interested in.

The first extensive experimental study is the one of Pumphrey *et al* in 1989 [7]. By dropping drops of water in a water bath with various drop diameters D and impact velocities U, they identified distinct zones with different mechanisms leading to bubble entrapment. Among them, they distinguish a regime they called *regular entrainment regime* as it was particularly reproducible. Other mechanisms exist that are also very reproducible [8]. In the following we focus on this regime, with droplets and liquid baths of the same liquid. We call it *pinching regime* as it is characterized by this mechanism of entrapment.

Typical images of this mechanism of bubble pinching are shown on the first row of figure 1 (the two other rows will be discussed later). A pure water droplet (diameter $D = 3$ mm) impacts the surface of a pure water bath with a velocity $U = 1.8$ m/s. The deformation of the interface is visualized by a high speed camera. In the first image (2.15 ms after the impact), the droplet has already entirely collapsed with the bath, and an air pocket (dark region) has started to develop. The second image (6.45 ms) shows the cavity during its expansion. It is roughly semi-spherical, with a wavy surface. The expansion is maximal at the third image (12.9 ms). Then the cavity starts to retract, taking a conical shape (4th image, at 18.3 ms) and finally pinching a bubble (19.15 ms) that is clearly detached on the last picture (20.16 ms). It is important to note that this pinching scenario is quite sensitive to the experimental parameters: for a given drop diameter, there is a narrow range of velocities that leads to bubble entrapment. For our example of a 3 mm-diameter

* Université Paris cité, CNRS, UMR 7057, Matière et Systèmes Complexes, 75013 Paris, France
† Sorbonne Université, CNRS, UMR 7190, Institut Jean Le Rond ∂'Alembert, F-75005 Paris, France
‡ Université Paris cité, CNRS, UMR 7057, Matière et Systèmes Complexes, 75013 Paris, France; caroline.derec@u-paris.fr

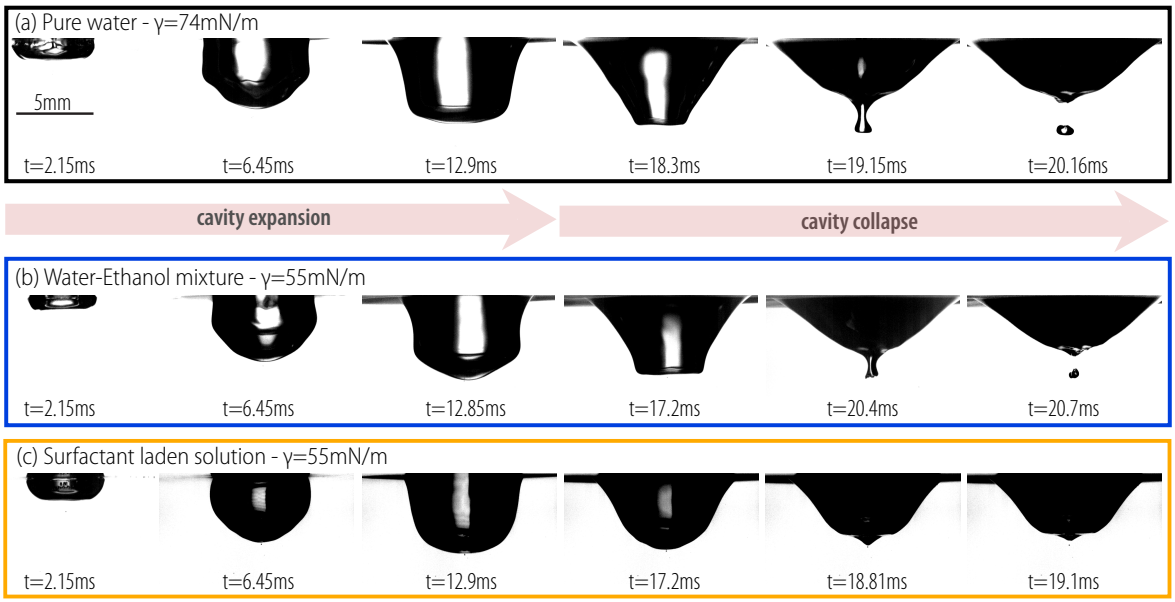

Figure 1. Sequences of cavities formed after drops impact on liquid interface, for $U = 1.8$ m/s. 1st row : distilled water $\gamma = 74$ mN/m, $D = 3$ mm. 2nd row : ethanol-water mixture $\gamma = 55$ mN/m, $D = 2.6$ mm. 3rd row : SDS solution $\gamma = 55$ mN/m, $D = 2.6$ mm. The third image of each sequence correspond to the maximum development of the cavity.

drop, a bubble is obtained for $1.2 < U < 2.2$ m/s. If the drop velocity is smaller or higher, the cavity collapse fails at pinching a bubble. Pumphrey *et al* [7] identified a delimited bubbling zone in the space of the parameters D, U. As the main forces involved in the process are gravity and surface tension, they proposed to re-plot the boundary of the bubbling region in terms of the Froude number Fr$= U^2/gD$, and the Weber number We$= U^2\rho D/\gamma$, where ρ is the liquid density, γ the surface tension and g the acceleration of gravity. With these numbers, the bubbling zone is well captured by two simple scaling laws [9]:

$$\text{We} = 48.3\text{Fr}^{0.247} \quad \text{for the upper limit,} \tag{1}$$

$$\text{We} = 41.3\text{Fr}^{0.179} \quad \text{for the lower one.} \tag{2}$$

Establishing a physical scenario that rationalizes these boundaries has attracted much attention. In their seminal work, Pumphrey *et al* [7] suggested that the capillary wave that travels down the sides of the crater may be the key of the mechanism. But they confess that "this is a speculative idea; attempts to use it to calculate when entrainment should occur have had only limited success." Oğuz and Prosperetti [9] proposed that the upper limit was given by a balance between a spreading radius R_{sp} and the crater radius R: if $R_{\text{sp}} > R$, the cavity grows radially and no bubble is entrapped. By estimating that $R_{\text{sp}} \sim D\text{We}$ and $R \sim D\text{Fr}^{1/4}$, they found an upper limit with an exponent remarkably close to the observations: We $\sim$ Fr$^{0.25}$. For the lower limit, they invoked a timing argument, between the period of the capillary wave t_w and the time to maximum growth of the crater t_{max}. Their reasoning leads to a We $\sim$ Fr$^{0.2}$, with an exponent 0.2 not far from the 0.179 observed. However, in their approach, they used a $t_{\text{max}} \sim DU^{1/3}$ scaling law (based on a private communication by Pumphrey) that, we shall see later, is not correct. It therefore appears that, more than thirty years after the law for bubble boundaries was empirically established, there is still no convincing physical scenario that accounts for it.

Many numerical studies have succeeded in reproducing the different stages of the cavity fairly accurately, from the droplet coalescence [10] to the cavity development [11], which can lead to the bubble detachment [12, 13]. Based on experiments and numerical simulation, different studies used an energy balance to obtain a differential equation for the cavity radius [11, 14, 15]. In a recent numerical study, Blanco-Rodriguez and Gordillo try to established a link between collapse of the cavity formed by capillary bubble floating at the surface of a liquid and the cavity collapse formed by drop impact [16]. They explore the role of the converging capillary waves toward the axis of symmetry in the succeeding jet. With an analytical approach, Longuet-Higgins noted that the pinch-off of the bubble can arise from a circular ripple converging on the vertex of a cone at a critical angle [17].

From an experimental standpoint, the properties of the liquid can strongly influence bubble production. In this context, the effect of viscosity has been studied both experimentally and numerically, comparing droplets and a liquid

bath with the same liquid [13, 18, 19]. These studies have shown that at higher viscosity, the bubbling regime shifts to higher impact velocities, up to disappearing. Recent research has also examined the behavior of drops falling into different liquids, such as viscous oil droplets and viscoplastic droplets falling onto water [20, 21]. However, in this paper, we have chosen not to focus on this particular configuration.

Our interest in the subject arose from the observation that the role of surface tension in bubble production had been little studied. When Pumphrey and Elmore proposed the Froude and Weber numbers to study the bubbling region, they wrote: "It would be very useful to know if the same effect occurred for other liquids and if the boundaries fell at the same values of We and Fr". It seems that this recommendation has been only partially followed up because to our knowledge very few authors looked into the role of surface tension. Pumphrey *et al.* [22] and recently Phillips *et al.* [23] mentioned an observation that adding washing-up liquid made the bubbling pinching regime disappear. Deng et al. [18] conducted experiments using a silicon oil with a low surface tension ($\gamma = 17.4\,$mN/m) and found a good agreement with the We-Fr relation.

In this study, we investigate systematically the effect of surface tension on bubble trapping in the pinching regime when a drop falls into a bath filled with the same liquid. We carried out experiments with two different systems for varying the surface tension of the solution: water-ethanol mixtures, and surfactant-laden solutions.

The second and third rows in figure 1 show how the cavity development is modified when the surface tension of the liquid is lowered (from 74 to 55 mN/m), in the case of an homogenous solution (water-ethanol, row 2), and a surfactant-laden solution (SDS, row 3). Note that the drops have the same impact velocity ($U = 1.8$ m/s), but are slightly smaller than in the pure water case ($D = 2.6\,$mm instead of 3 mm), because they detach earlier from the capillary used to produce them. For the water-ethanol mixture, the general sequence is similar to the one for water: the cavity expansion reaches its maximum at the same time and with approximately the same depth, there is a conical shape, and a bubble is pinched at the end of the collapse. There are, however, some notable differences: the waves on the cavity are less pronounced at the beginning (second image), the time of the pinching is increased, and the trapped bubble is smaller. For the Sodium Dodecyl Sulfate (SDS) solution, the sequence is strikingly different: the surface of the cavity is smoother (no waves), there is no conical shape, and the final pinching fails at trapping a bubble. These observations suggest that the capillary waves is one of the key features driving for the bubbling process.

After describing the experimental set-up as a whole (Sec.II), we first explore the influence of the properties of the different liquids on the development of the cavity (Sec.III). Next we will focus on the conditions under which the bubble detaches, looking at the effects of surface tension and viscosity (Sec.IV,V). This study will lead us, in the final section, to examine the role of the damping of the capillary wave on the bubbling regime (Sec.VI).

II. EXPERIMENTAL SETUP

The experiment consists in dropping a single droplet at heights ranging from 5 to 60 cm into a tank filled with the same liquid. The objective is to record the shape of the submerged cavity formed upon impact and the underwater noise generated during the collapse of the cavity. Figure 2a illustrates the experimental setup. The droplet falls in a plexiglas tank ($15\,$cm$\times 15\,$cm section, $6\,$cm depth) filled with either pure water, an aqueous ethanol solution or an aqueous solution of Sodium Dodecyl Sulfate surfactant (SDS - purchased from Sigma Aldrich). In the aqueous ethanol solutions, the weight fraction of ethanol varies from 5 to 100 %. In the aqueous SDS solutions, the mass concentration ranges from 0.1 mM to 15 mM. For SDS at the ambient temperature, the critical micellar concentration (CMC) is around 8.1mM [24–26]. Droplets are generated using a syringe with a 22G needle (external diameter $2a = 0.72\,$mm), attached to a syringe pump itself mounted on a translation stage for precise variation of the drop height H. The impact velocity U is related to the height through the relation $U = \sqrt{2gH}$, where g is the acceleration of gravity. This equation introduces a maximum error of $4\,\%$ for our specific range of drop diameters and heights. For each solution, the drop diameter D is calculated by weighting approximately 100 drops, assuming they are spherical. Since we maintain a constant needle size, the effect of the surface tension in ethanol and SDS solutions causes D to vary within the range of 2 to 3 mm. By knowing the drop diameter and the external needle diameter, the surface tension of the solution is calculated using an approximate balance that relates the gravitational force pulling the drop down to the surface tension force at the instant of drop detachment: $\beta 2\pi\gamma a = (4/3)g\pi\rho(D/2)^3$, with $\beta = 3.60/(2\pi)\left((\pi/6)^{1/3}D/a\right)^{0.19}$ [27]. Figure 2 displays the surface tension as a function of concentration for ethanol and SDS aqueous solutions. Our measurements are in a good agreement with the literature. In the inset of figure 2a we provide the values of the viscosity for ethanol-water mixture, extracted from [28]. It is also important to note that the viscosity varies from 1 to 3 mPa.s. Table I reports the range of liquids properties and drop sizes used in this work.

After the impact, the cavity undergoes expansion before collapsing, occasionally resulting in the entrapment of a small bubble, as shown in fig. 1. These complex interfacial reconfigurations are analyzed through close-up high-speed

Liquid	γ (mN/m)	η (mPa/s)	ρ (kg/m^3)	D (mm)
Distilled water	74-69	1	1000	3
Ethanol-Water mixture	60-24	1-3	780-1000	2-3
SDS Solution	70-35	1	998	2.4-3

Table I. Range of variations of the properties for the liquids used in this study.

imagery using a macro lenses mounted on a digital high-speed camera (Phantom V9.1) at 3720 frames per second.

An hydrophone (B&k 8103 - flat bandwidth $[2-20]$ kHz) is placed in the tank. It is connected to an homemade amplifier and a digital oscilloscope (TiePie). When a bubble is entrapped, it resonates at its fundamental mode, so-called Minnaert resonance [29], and a strong acoustic signature is recorded. We use this acoustic signal to determine whether the impact entrapped a bubble or not.

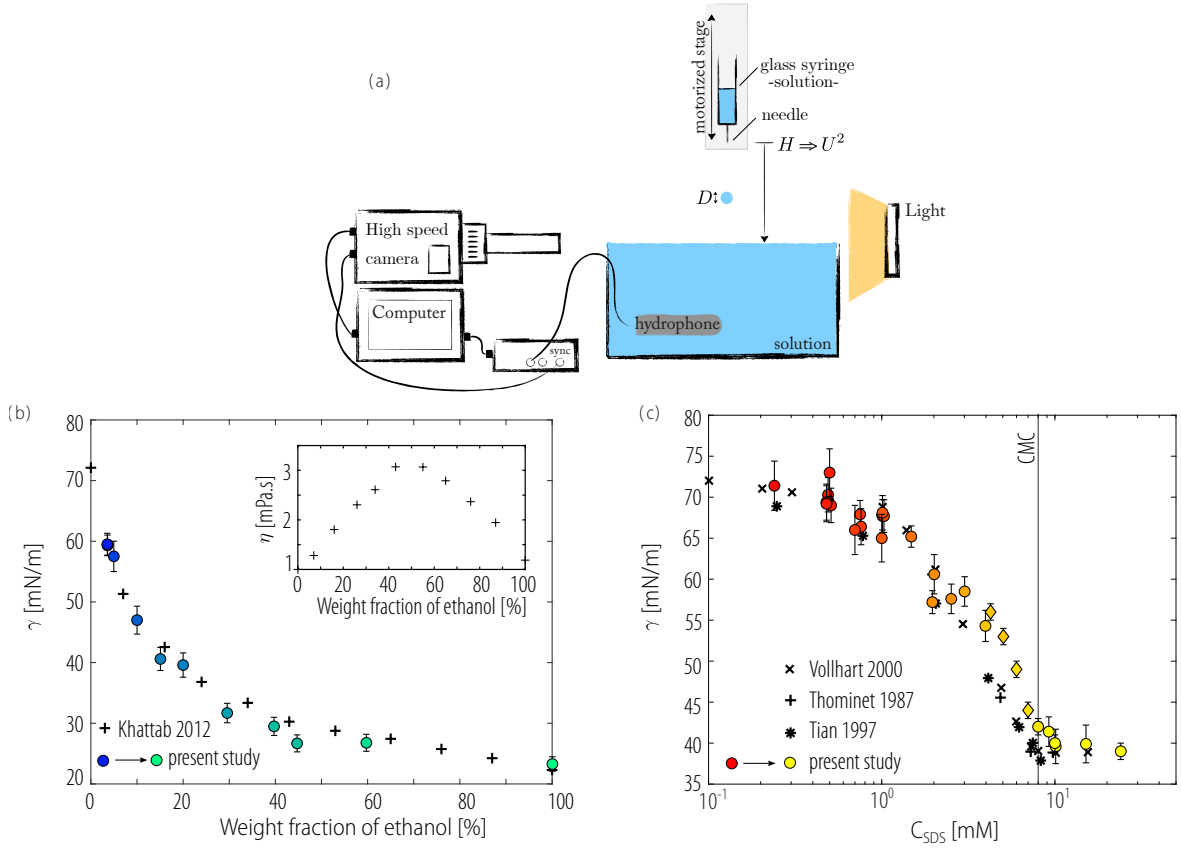

Figure 2. (a) Sketch of the experimental setup. (b) **Surface tension as a function of mass fraction of ethanol for ethanol mixtures**. Colored circles : present study. Colors from blue to green code for the ethanol concentration. '+': data from Khattab 2012. Insert: viscosity from Khattab 2012 [28]. (c) **Surface tension as a function of SDS concentration in pure water**. Colors circles and diamonds from red to yellow code for the SDS concentration. Diamond markers code for concentrations where no bubbles are trapped. 'x': data from Vollhardt 2000 [26]. '+': data from Thominet 1987 [25]. '*': data from Tian 1997 [24]. Note that the color code for the ethanol solutions and the SDS solutions will be the the same in the following figures.

III. CAVITY EXPANSION: EFFECT OF SURFACE TENSION

In this first part, we focus on the expansion of the cavity. Our aim is to determine whether the experiments with liquids of different surface tensions lead to differences in the cavities.

Figure 3a shows typical images of the cavities, here for pure water drops at two different impact velocities: $U = 2$

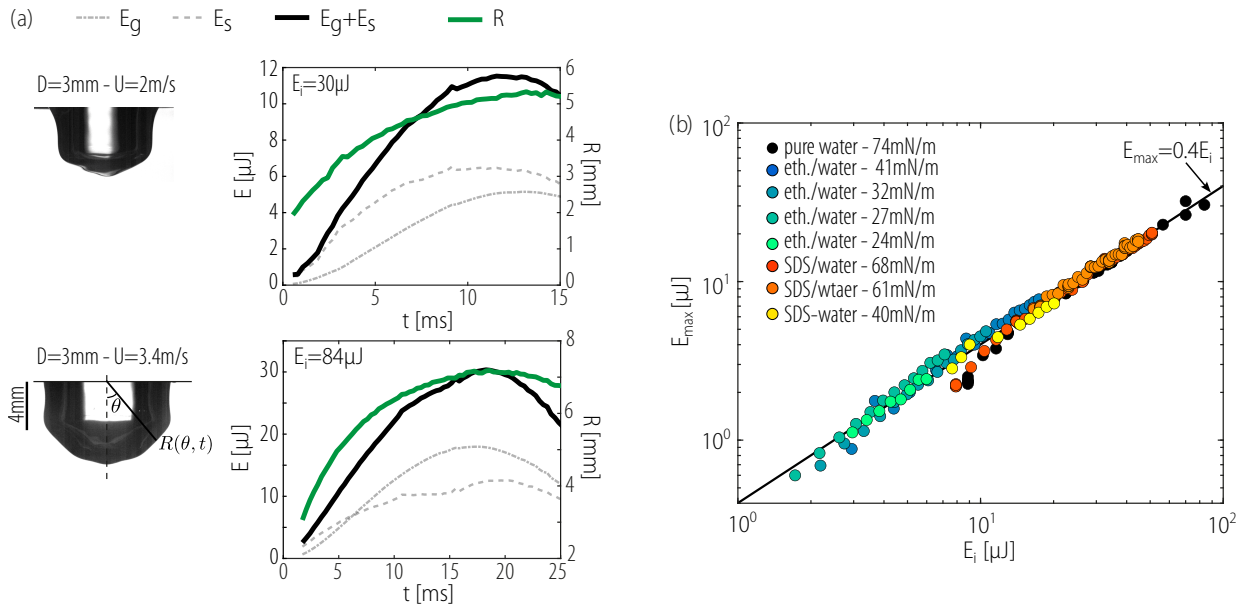

Figure 3. (a) Snapshots of cavities, at their maximal development, for water drops ($D = 3$ mm) with 2 different impact velocities: 2 m/s and 3.4 m/s. From image analysis, we can estimate the potential energies (black) and equivalent radius (green) of the cavities, as functions of time. (b) Maximum potential energy of the cavity $E_{\max}$ as a function of the impact energy E_i. The line represents a ratio of 40%.

and 3.4 m/s. Given the axial symmetry of the cavities, we can easily extract three quantities from the image analysis at each time: the equivalent radius defined from the polar angle θ (see Fig.3a)

$$R = \frac{1}{\pi}\int_{\theta=-\pi/2}^{\theta=\pi/2} R(\theta)d\theta, \tag{3}$$

the surface energy

$$E_s = \gamma\left(\int_{z=0}^{z_{\max}} 2\pi r(z)dz \; - \pi r(0)^2\right) \tag{4}$$

and the gravitational energy

$$E_g = \int_{z=0}^{z_{\max}} \rho g\, \pi r^2(z) z\, dz \tag{5}$$

where $z = R\cos\theta$ and $r = R\sin\theta$.

Figure 3a reports these quantities as functions of time for the two examples. Note that the two potential energies are of the same order of magnitude: one cannot neglect one compared to the other. The total potential energy (thick black lines) goes through a clear maximum, which we will use to define $t_{\max}$, the maximal expansion of the cavity. We note $R_{\max}$ the equivalent radius of the cavity at that time, and $E_{\max}$ its total potential energy.

An interesting parameter, which combines the effect of surface tension, size and velocity, is the impact energy

$$E_i = \pi\rho D^3 U^2/12 + \pi\gamma D^2. \tag{6}$$

E_i is the sum of the kinetic and surface energy of the impacting drop. It ranges from a few μJ to almost 100 μJ in our experiments. We see on the two examples of figure 3a that all the impact energy is not converted into potential energy : $E_{\max}$ is always less than E_i. This is confirmed in figure 3b which reports $E_{\max}$ as a function of E_i for all our experiments, with different impact velocities and liquids. We find that all the data reasonably collapse on a straight line with a slope of 0.4. It means that only 40% of the impact energy is stored as potential energy in the cavity. The rest of the energy is probably under the form of kinetic energy of the displaced fluid in the volume and surface wave

energy at the surface of the liquid bath. Note that viscous dissipation is probably low because the ethanol solutions follow the same law, even if their viscosity varies over a factor 3 when the concentration varies. We also note that previous studies in the literature reported different ratios of $E_{\max}/E_i$, typically from 60 to 80 % [9, 14, 19, 30, 31]. But they approximated the cavity by a cylinder or an hemisphere, whereas we analysed its exact shape. A recent article by Lherm et al [15] finds the same ratio of 40% using the same approach as us.

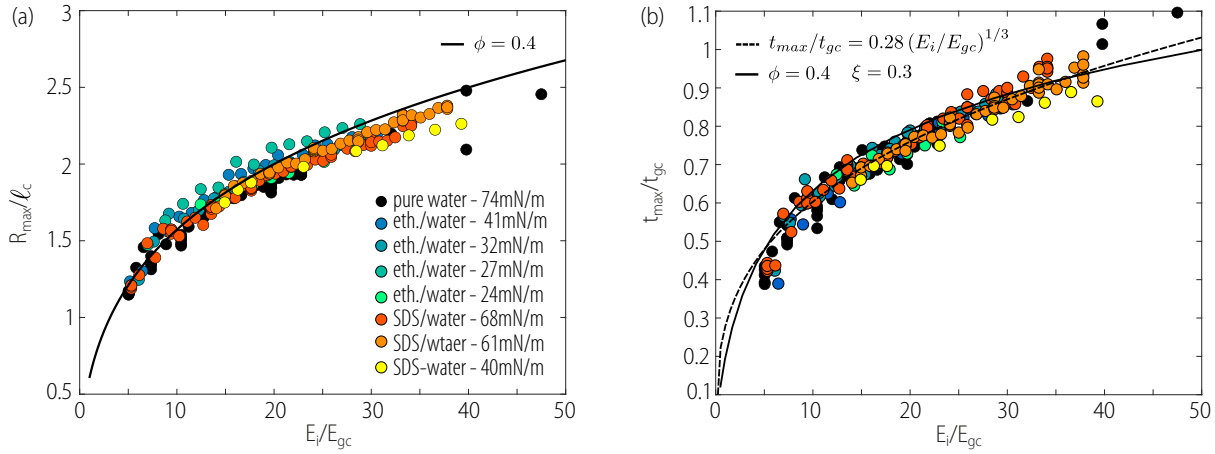

Figure 4. (a) Equivalent radius at the maximum potential energy $R_{\max}$ rescaled by the capillary length $\ell_c = \sqrt{\gamma/(\rho g)}$ as a function of E_i/E_{gc}, with $E_{gc} = \pi\gamma^2/(\rho g)$. The solid line represents equation (8) using $\phi = 0.4$. (b) Time at the maximum energy $t_{\max}$ rescaled by the time $t_{gc} = (\gamma/(\rho g^3))^{1/4}$ as a function of E_i/E_{gc} . The solid line represents a numerical resolution of Eq. (7) using $\xi = 0.3$ and $\phi = 0.4$. Dashed line corresponds to the best fitting power law.

We can try to model the dynamics of the cavity by making the crude assumption that it behaves as an hemisphere with radius $R(t)$. We can write that the total energy is conserved:

$$\phi E_i = \gamma\pi R(t)^2 + \frac{1}{4}\rho g\pi R(t)^4 + \xi\rho\pi R(t)^3\dot{R}(t)^2. \tag{7}$$

Parameter ϕ accounts for the fraction of the impact energy that is effectively converted into the expansion of the cavity. Parameter ξ was proposed by Lherm et al [15] to account for the fact that the true velocity field is not purely radial. A true hemisphere expansion would be with $\phi = \xi = 1$. In our case, we have seen that $\phi = 0.4$ and we will use ξ as a fitting parameter.

The maximum expansion of the cavity is given by Eq. (7) for $\dot{R} = 0$, which leads to

$$R_{\max} = \sqrt{2}\ell_c\sqrt{\sqrt{1 + \frac{\phi E_i}{E_{gc}}} - 1} \tag{8}$$

where $\ell_c = \sqrt{\gamma/(\rho g)}$ is the capillary length, and $E_{gc} = \pi\rho g\ell_c^4$ is a gravito-capillary energy. Figure 4a confirms that plotting $R_{\max}/\ell_c$ as a function of E_i/E_{gc} collapses all the experimental data on a master curve, which is well captured by Eq. (8) with $\phi = 0.4$ (black line). Note that equation (8) suggests that $R_{\max}$ depends on the surface tension, via ℓ_c and E_{gc}. Yet, interestingly, at the limit of high impact energy, this dependency disappears:

$$R_{\max} \simeq \left(\frac{4\phi E_i}{\pi\rho g}\right)^{1/4} = D(\phi\mathrm{Fr}/3)^{1/4} \quad \text{for} \quad \sqrt{\frac{\phi E_i}{E_{gc}}} \gg 1. \tag{9}$$

In practice, this limit of high impact energy is easily reached, which justifies the $R/D \sim \mathrm{Fr}^{1/4}$ law often used in the literature [9, 15, 31, 32] for estimating the size of the cavity.

From Eq. (7) we can also estimate the time of maximum energy, $t_{\max}$. Dimension analysis suggests that gravito-capillary time $t_{gc} = (\gamma/(\rho g^3))^{1/4}$ is involved. Indeed, as shown in figure 4b, all the data collapse reasonably well when $t_{\max}/t_{gc}$ is plotted as a function of E_i/E_{gc}. Numerical resolution of the equation with $\phi = 0.4$ and $\xi = 0.3$ leads to a good master curve for all the results. Lherm et al. [3, 15] recently found similar results with a slighlty larger

value of $\xi = 0.35$. Note that this master curve may be fitted by the power law $t_{max}/t_{gc} = 0.28(E_i/E_{gc})^{1/3}$ (see dashed line in Fig. 4b). This leads to the relation $t_{max} \propto DU^{2/3}$, which is in contradiction with the power law $DU^{1/3}$ invoked by Oguz and Prosperetti to justify the Fr-We law, as mentioned in section I.

As a conclusion on this first part, we have found that 40% of the impact energy was converted into potential energy, and we confirmed that a simple model of an hemi-spherical cavity was sufficient to capture the maximum size, and the time at which this size was reached. Interestingly, there is no distinction between the water-ethanol mixtures and the SDS solutions. We shall see that the situation is different for the bubbling region.

IV. EFFECT OF SURFACE TENSION ON THE BUBBLING ZONE

As the entrapped bubbles make a loud noise, we used the acoustic signal recorded by the hydrophone to determine whether an impact led to a bubble or not. For each solution, multiple impacts (at least 20) were performed at each height, and we considered that we were in the bubbling zone when at least 50% of the impacts resulted in a clear acoustic signal. Figure 5a shows the resulting diagram of bubbling in the (U,γ) space, for the two kinds of solutions we used. In water-ethanol mixtures, the upper limit of the bubbling regime decreases when the surface tension decreases, while the lower limit remains roughly flat. For SDS solutions, the picture is very different. As soon as a small amount of SDS ($\approx$ CMC/10) is added to water, the bubbling zone is strongly shifted towards larger impact velocities. Remarkably, there is an area between $\gamma = 42$ mN/m and $\gamma = 55$ mN/m where no bubble are pinched. This empty zone corresponds to concentrations in surfactant between 0.5 CMC and 1 CMC. At the CMC and above, the bubble entrapment regime reappears, with a width similar to that of ethanol for the same surface tension, but for higher impact velocities. As already evidenced in figure 1, it means that surface tension is clearly not sufficient to predict the entrapment of a bubble by the cavity collapse.

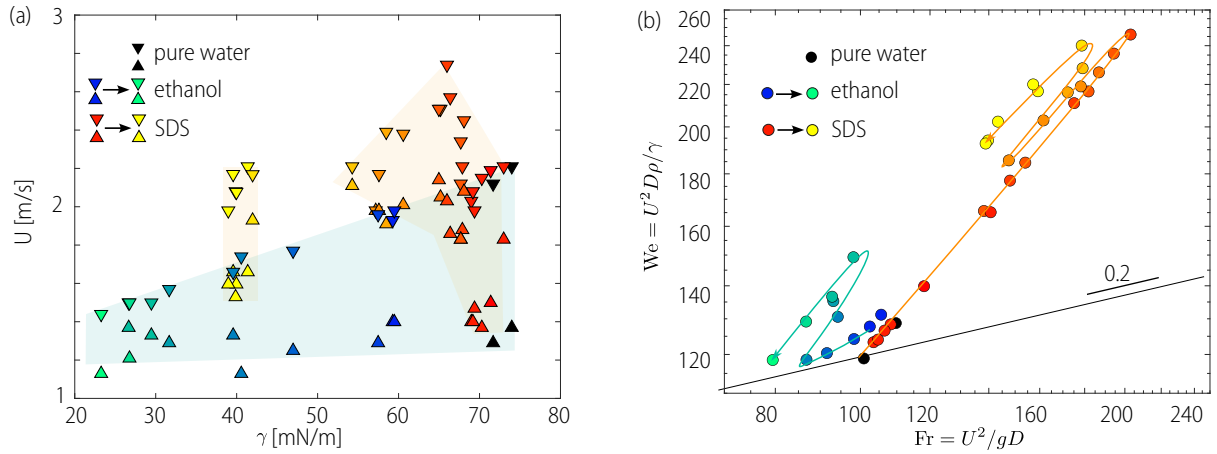

Figure 5. (a) Bubble pinch-off diagram U-γ. Up-triangles indicate the beginning of bubbling zone and down-triangles its end (when increasing the impact velocity U). The light blue and the light orange areas are guides for the eye to highlight the bubbling zones. (b) Bubbling line (i.e. centre of the bubbling zone considering the velocity) in a Weber-Froude representation. The straight black line We$= 45\mathrm{Fr}^{0.2}$ is the bubbling line extracted from the data of Pumphrey and Elmore [22] for pure water. Colored curved lines are guides for the eye following the increasing concentration in ethanol and SDS.

Figure 5a diagram is not a perfect slice in the (U,D,γ) space, because D is not constant. As all the drops were obtained with the same needle, the drop size decreases when γ decreases (D varies in $\gamma^{0.36}$). To consider the combined effect of U,D and γ, we look at our measurements in a We-Fr diagram. In the following, instead of plotting the lower and upper boundaries, we will consider only the middle of the bubbling zone (defined as the mean velocity between the low and high velocity frontiers), which we will call the *bubbling line*. Physically, the bubbling line has a particular role, as it corresponds to the points where the size of the trapped bubbles is maximal [13, 22]. Furthermore, this choice will allow a comparison with data from the literature (see next Section) where the definition of the width of the bubbling zone is not specified. Figure 5b reports our data in such a representation. For comparison, we also plot We$= 45\mathrm{Fr}^{0.2}$ (solid line) which is a reasonable law for the bubbling line we extracted from the experimental data found by Pumphrey *et al* for water drops falling in a water bath [7, 22]. It means that, if We and Fr were the only

parameters involved in the problem, one would expect all the data to collapse on this line. Clearly, there are strong deviations for SDS solutions. But, more surprisingly, water-ethanol mixtures also deviate from what is expected: the low and high concentrations remain close to the Pumphrey bubbling line, but intermediate ones are quite far. As water-ethanol mixtures are known to exhibit a peak in viscosity for intermediate concentrations (see inset of figure 2), this observation led us to consider a possible effect of viscosity.

V. EFFECT OF VISCOSITY ON THE BUBBLING REGION

Several studies have been conducted to understand the effect of viscosity on the bubbling zone [13, 18, 19]. We extracted experimental and numerical data from the literature (see table II) to obtain the bubbling lines in the We-Fr space. Figure 6a depicts all of these data. It clearly shows that measurements with identical drop sizes deviate from the We-Fr law and instead form straight lines that appear parallel to our data.

Reference	exp/num	γ (mN/m)	η (mPa/s)	ρ (10^3 kg/m^3)	D (mm)
Pumphrey1989 [7]	exp	72	1	1	1-5
Deng2007 [18]	exp	[69.2, 67.2, 63.9]	[5.9, 10.2, 14.7]	[1.126, 1.153, 1.172]	[1.5-3.29]
Michon2017 [19]	exp	[70, 70, 67, 64, 64, 64]	[1.12, 1.18, 2.5, 6, 12.5, 15]	[1, 1.03, 1.06, 1.14, 1.17, 1.2]	2.7
Chen2014 [13]	num	72	[0.1, 0.5, 1, 2.5, 5, 7.5, 10, 14.7]	1	[1.8, 2.36, 2.8]

Table II. Liquid properties and drop diameters for the data extracted from literature (see figure 6). The second column indicates whether the reference is an experimental (exp) or numerical (num) study.

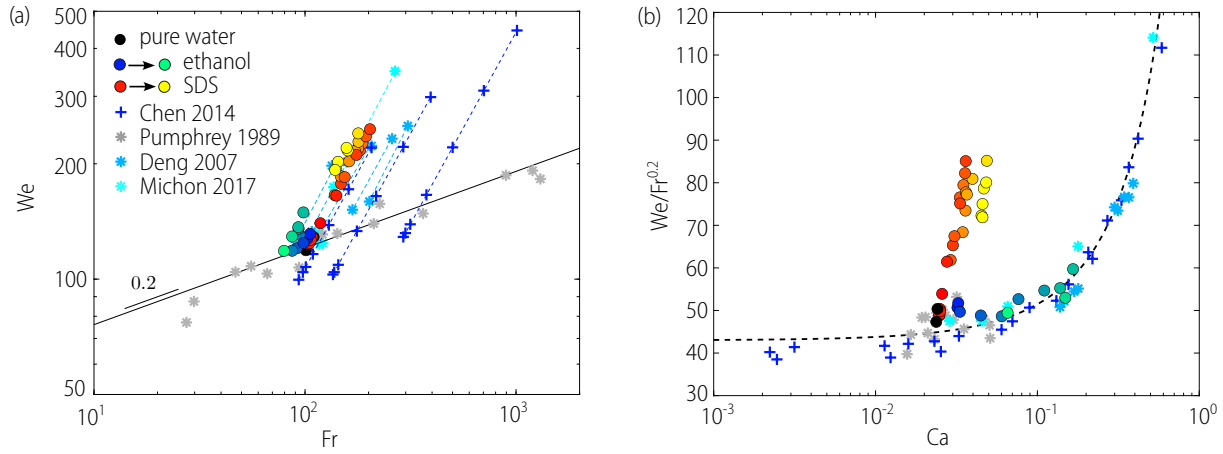

Figure 6. **Dimensionless bubbling line**. (a) Weber number We=$U^2\rho D/\gamma$ as a function of the Froude number Fr=$U^2/(gD)$. The black line represents the empirical law We= $45\text{Fr}^{0.2}$. The dotted lines connect points from experiments with the same drop diameters and different viscosities. (b) Ratio We/Fr$^{0.2}$ as a function of the capillary number of the droplet Ca=$\eta U/\gamma$. The black dashed line represent the empirical law We/Fr$^{0.2}$ = 43exp(1.8Ca). In (a) and (b) when possible, data were extracted from the literature [7, 13, 18, 19] (see Tab. II).

To incorporate viscosity in the space of parameters, several dimensionless numbers can be considered: Reynolds number Re= $DU\rho/\eta$, Laplace number La= $\gamma\rho R/\eta^2$ or Capillary number Ca= $U\eta/\gamma$. Relying on the scaling law We $\propto$Fr$^{0.2}$ which depicts well the water case, we have tested a large number of combinations and we found that the Capillary number was the best quantity allowing to collapse all the data collected from the literature and our experimental measurements with ethanol (see figure 6b). If we do not consider the measurements with the surfactant-laden solutions, one can define a purely empirical law describing the bubbling line:

$$\frac{\text{We}}{\text{Fr}^{0.2}} = 43\exp(1.8\text{Ca}). \tag{10}$$

Note we do not have a physical explanation to date for the presence of the exponential. However, this empirical law has the advantage of accounting for the observation of a limiting viscosity, beyond which bubbling is never observed

for a given drop diameter, whatever the impact velocity. For instance, Deng et al. reported that no bubbles were detached for drops with diameter varying between 1.5 and 3.29 mm using water-glycerin mixtures with $\rho = 1.2$ g/cm^3, $\gamma = 64$ mN/m and $\eta = 15$ mPa.s. Michon *et al.* [19] confirmed this observation with 2.7 mm drops. With these set of parameters D, ρ, γ and η one can check that there is no solution in U that satisfies equation (10) (see Appendix A).

At this stage, we have obtained a first conclusion concerning the effect of surface tension and viscosity on the bubbling regime: for homogeneous solutions, such as water-ethanol mixtures and water-glycerin mixtures, it appears that We-Fr law works, providing that the effect of viscosity is also taken into account, via empirical law (10).

One effect of the viscosity can be observed by comparing the second image of the first two lines of Fig. 1, where the cavity appears smoother in the case of the water-ethanol solution. Still looking at Fig. 1, if we now consider the case of surfactant-laden solutions, we can see that the cavity is even smoother. This observation suggests that capillary waves play an important role.

VI. CAPILLARY WAVE DAMPING WITH SURFACTANT MOLECULES

To quantify the effect of surfactant molecules in our experiments, we calculated the capillary number that was needed to reconciliate the SDS bubbling line with the empirical law (10). In other words, we projected the SDS data points on the empirical curve in Fig. 6b. We thus obtained an effective Capillary number, which could be converted into an effective ratio between the viscosity and surface tension η/γ. The result of this "projection" is shown in Fig 7, which presents $(\eta/\gamma)_{\text{eff}}$ as a function of the concentration in SDS (colored circles). We can go a step further, and compare these results to independent measurements of capillary wave attenuation in SDS solutions. Noskov and Grigoriev [33] measured the attenuation α (inverse of the attenuation length) associated with planar linear capillary waves propagating on a plane interface of SDS solution. We thus report in the same figure the effective ratio $(\eta/\gamma)_{\text{eff}}$ and the attenuation α they measured for such planar waves excited at a frequency $\omega/2\pi$ = 200 Hz, for various SDS concentrations (blue crosses).

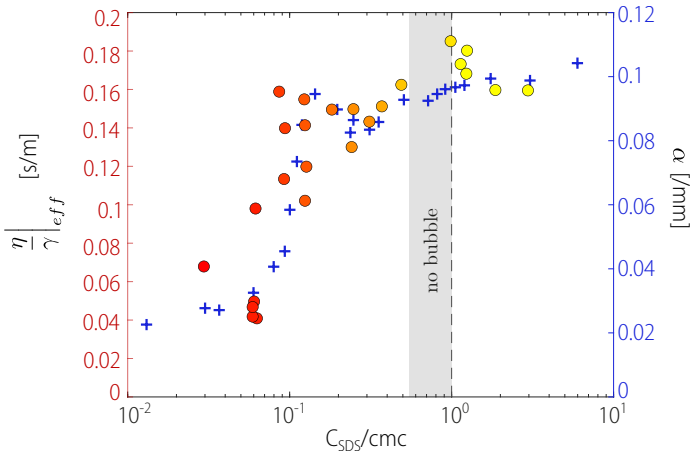

Figure 7. **Capillary waves attenuation**. Left axis, full circles : effective ratio η/γ of SDS solution (eq. 10) as a function of the SDS concentration C_{SDS} adimentionned by the CMC. Right axis, blue crosses: Attenuation α of planar capillary waves at 200Hz measured at the surface of SDS solutions as a function of the SDS concentration (data extracted from [33]).

The two curves show a remarkably similar pattern, with a sharp increase at a concentration about CMC/10. To take a step further the comparison between the effective attenuation obtained from the bubbling mechanisms and the damping of plane capillary waves measured by [33], numerical values are compared. First let us note that the wavelength associated with plane waves excited at 200 Hz (around 2 mm) is close to the drop diameter in our experiment. Using the relation for planar waves between attenuation and liquid viscosity in the case of viscous damping: $\alpha = (4/3)\omega\eta/\gamma$, the damping measured in [33] is converted into a measure of the quantity $(\eta/\gamma)_{\text{eff}}$. We found only a factor 3 of difference with our values, which is remarkably close although with completely different experimental setup and geometry: in one case, there are plane waves propagating on a flat interface, while in the other, there are converging circular waves propagating on a curved interface. These observations reinforce the idea that capillary waves play a crucial role in bubbling mechanisms.

This sharp increase in damping even at low concentration is consistent with the work of Lucassen and Hansen [34, 35] who demonstrated the role of surfactant dynamics in damping the surface waves, thus acting as an effective viscosity. As waves locally stretch or compress the interface, they lead to locally lower or higher surfactant concentration, and the resulting surface tension gradients induce tangential shear forces, called Marangoni forces. These lead to an additional flow and thus to some additional damping effect. With insoluble surfactants, the damping is directly related to the Gibbs-Marangoni modulus which links the surfactant surface concentration and the interface compression. The surfactant solubility becomes non-negligible when the characteristic times of the wave becomes comparable to the characteristic times of surfactants exchange between the interface and the bulk, and the resulting modification of the surface rheology influences in a complex manner the damping of the capillary waves [33–36].

The manifestation of such strong effect of the presence of surfactants even at very low concentration is consistent with previous observations on complex hydrodynamic phenomena. In an identical geometry, Constante-Amores *et al.* [37] studied numerically the effect of surfactants on the dynamics of a bubble bursting. They observed how the circular capillary wave is covered with surfactants, and how surfactant gradients are becoming larger and larger when the wave converges at the bottom of the collapsing cavity. They showed that these gradients lead to Marangoni flows strong enough to influence the Worthington jets emitted after the collapse. Erinin *et al.* [38] have studied the effects of surfactants on a mechanically generated plunging breaker. The experiments have revealed that the presence of surfactants can strongly alter the dynamics of the plunging breakers, with a particularly strong effect at low concentrations of surfactants. The authors observed numerically that the surface tension gradients are maximal at the wave crest, thus leading to strong Marangoni stresses that alter the wave breaking process, especially at low surfactant concentration.

These observations are consistent with the peak of attenuation detected in our experiments at low concentration about CMC/10. In this context, we speculate that the disappearance of bubbling at intermediate concentrations just before the CMC (colored area in Fig. 7) should correspond to the emergence of another significant attenuation peak, which would not be detected in linear plane wave experiments. The existence of such an attenuation peak needs to be experimentally confirmed and explained, which is beyond the scope of this paper. This observation is compatible with the remarks of Prosperetti et al. and Philips et al. [23, 39] who reported seeing no bubbling when surfactant is added to water. Our hypothesis is that the solutions they chose had a too high surface elasticity, which is common with a washing-up liquid.

VII. CONCLUSION

Drop impact experiments on a liquid bath were carried out by varying the surface tension γ of the liquid, using pure water solutions, water-ethanol and water-SDS mixtures at different concentrations. The objective was to explore the influence of surface tension on bubble entrapment in the pinch-off regime. Following the pioneering work by Pumphrey et al [7] we constructed a *bubbling diagram* in the plane (γ, U) (i.e. surface tension, drop impact velocity) and shown that the velocity range for bubble entrapment varies with surface tension in the water-ethanol solutions at different concentrations. Notably, the conditions for bubbling in water-SDS solutions remain distinctly different, even at the same surface tension values than for ethanol mixtures, indicating that surface tension alone is not the sole relevant parameter.

To elucidate the solution properties that play a role in bubbling and understand the underlying mechanisms, our initial focus centered on the cavity development phase, exhibiting a dependence on both U and γ. Through analyses of cavity profiles, we measured the gravity and surface potential energy of the cavity during its development. Notably, at maximum cavity development, we found that only 40 $\%$ of the drop impact energy is converted into potential cavity energy, for all tested solutions, with surface tension from 24 to 72 mN/m and viscosity approximately ranging from 1 to 3 mPa.s. This suggests that the remaining energy is predominantly converted into kinetic energy in the liquid bath. Furthermore, our findings revealed that the characteristic size and development time of the cavity follow a master curve when plotted against drop impact energy, all these quantities being rescaled by gravito-capillary quantities. Additionnally, a naive model of cavity growth considering only the impact energy and gravito-capillary parameters provided a satisfactory description of the experimental observations. This validates the idea that the development phase alone can not explain the conditions leading to bubble pinch-off.

The measurements establishing the bubbling zones in the (U, γ) plane were compared with the scaling law $\mathrm{We} \propto \mathrm{Fr}^{\alpha}$ frequently used in the literature for water. We also compiled a large number of experimental and numerical data from the literature, including a wide range of viscosity variations. It turns out that, as long as the viscosity of the solutions is close to that of water, the We-Fr scaling law correctly describes the data as surface tension varies. However, as viscosity increases, it must be considered and we have shown that the empirical law $\mathrm{We} \propto \mathrm{Fr}^{0.2} \exp(1.8\mathrm{Ca})$,

with the capillary number Ca $=\eta U/\gamma$, satisfactorily describes bubbling conditions taking all parameters (γ, ρ, η) into account. Considering that the capillary number is characteristic of the viscous damping of a capillary wave, we have introduced an effective value for the quantity η/γ for water-SDS solutions, thus reconciling their behavior with that of solutions without surfactant molecules. Our hypothesis is that this effect arises from capillary wave damping induced by Marangoni effects due to the presence of surfactant molecules. This approach confirms the fundamental role of capillary waves propagating along the cavity surface in bubble trapping mechanisms.

This work can be compared with *bubble bursting* experiments, revealing a striking similarity with cavity retraction after drop impact. Both scenarios involve the propagation of a wave along the cavity surface before retraction [16]. Recent investigations [37, 40, 41] have explored the influence of interfacial molecules, for example on droplet production from the liquid jet expelled after cavity retraction. Notably the presence of SDS has been linked to the generation of smaller and faster droplets, while concentration about CMC/2 result in their disappearance [41], again demonstrating the complex effects of surfactant molecules in these fast hydrodynamic phenomena.

Appendix A: Critical viscosity predicted by the bubbling line

Empirical law (10) can be used to determine a critical viscosity, above which no bubble can be entrapped. Indeed, for a given liquid and droplet diameter, one can determine the speed for which bubbling is obtained by rewriting (10) as

$$U^{1.6} = f(U) = \frac{43\gamma}{\rho D^{1.2} g^{0.2}} \exp(1.8U\eta/\gamma), \tag{A1}$$

which can be solved graphically. Figure 8 shows two examples of graphical resolutions, related to two experimental situations explored by Michon and coworkers [19]. For a viscosity of 1 mPa.s, there is a solution. But for 15 mPa.s the two curves do not intersect, which is consistent with the experimental observations: for this viscosity, no bubble was observed whatever the velocity of the drop. Note here that while other empirical laws would also satisfactorily fit the experimental data in Fig. 6b, the exponential law has the advantage of being a simple law that additionally is consistent with the existence of this critical viscosity, which is not the case, for example, with a linear law.

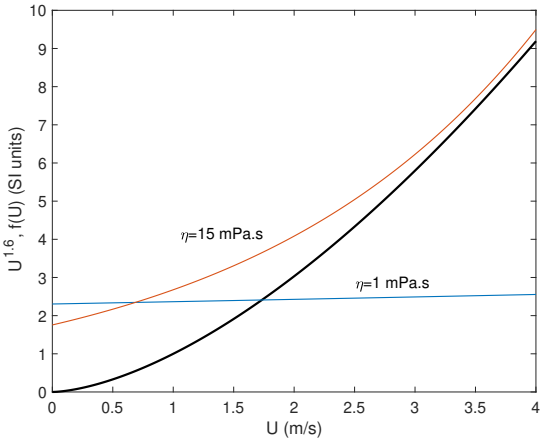

Figure 8. **Graphical resolution of (A1).** The intersection of $U^{1.6}$ (black curve) and $f(U)$ (blue and red curves) gives the value of the velocity U for which bubbling is expected.

[1] R S Cole A M Worthington. Impact with a liquid surface, studied by the aid of instantaneous photography. Philosophical Transactions of the Royal Society of London, 189, Aug 1897.
[2] H.E. Edgerton and J.R. Killian. Flash ! Seeing the Unseen by Ultra High-speed Photograph. Branford, Boston, 1954.
[3] V. Lherm, R. Deguen, T. Alboussière, and M. Landeau. Rayleigh-taylor instability in impact cratering experiments. Journal of Fluid Mechanics, 937, feb 2022.

[4] Fabrice Veron. Ocean spray. Annual Review of Fluid Mechanics, 47(1):507–538, 2015.

[5] Luc Deike. Mass transfer at the ocean–atmosphere interface: The role of wave breaking, droplets, and bubbles. Annual review of fluid mechanics, 54:191–224, 2021.

[6] A Prosperetti and H N Oguz. The impact of drops on liquid surfaces and the underwater noise of rain. Annual Review of Fluid Mechanics, 25(1):577–602, 1993.

[7] Hugh C Pumphrey, LA Crum, and L Bjo/rno/. Underwater sound produced by individual drop impacts and rainfall. The Journal of the Acoustical Society of America, 85(4):1518–1526, 1989.

[8] G. Gillot, C. Derec, J.-M. Génevaux, L. Simon, and L. Benyahia. A new insight on a mechanism of airborne and underwater sound of a drop impacting a liquid surface. Physics of Fluids, 32(6):062004, Jun 2020.

[9] Hasan N Oguz and Andrea Prosperetti. Bubble entrainment by the impact of drops on liquid surfaces. Journal of Fluid Mechanics, 219:143–179, 1990.

[10] Francois Blanchette and Terry P. Bigioni. Partial coalescence of drops at liquid interfaces. Nat Phys, 2(4):254–257, 04 2006.

[11] Edin Berberović, Nils Van Hinsberg, Suad Jakirlić, Ilia Roisman, and Cameron Tropea. Drop impact onto a liquid layer of finite thickness: Dynamics of the cavity evolution. 79.

[12] David Morton, Murray Rudman, and Liow Jong-Leng. An investigation of the flow regimes resulting from splashing drops. Physics of Fluids (1994-present), 12(4):747–763, 2000.

[13] Senlin Chen and Liejin Guo. Viscosity effect on regular bubble entrapment during drop impact into a deep pool. Chemical Engineering Science, 109:1–16, 2014.

[14] Olive G Engel. Crater depth in fluid impacts. Journal of Applied Physics, 37(4):1798–1808, 1966.

[15] V. Lherm and R. Deguen. Velocity field and cavity dynamics in drop impact experiments. Journal of Fluid Mechanics, 962, apr 2023.

[16] Francisco J. Blanco Rodriguez and J. M. Gordillo. On the jets produced by drops impacting a deep liquid pool and by bursting bubbles. Journal of Fluid Mechanics, 916, apr 2021.

[17] M. S. Longuet-Higgins. An analytic model of sound production by raindrops. J. Fluid Mech., 214:395–410, 1989.

[18] Q. Deng, A. V. Anilkumar, and T. G. Wang. The role of viscosity and surface tension in bubble entrapment during drop impact onto a deep liquid pool. Journal of Fluid Mechanics, 578:119–138, apr 2007.

[19] Guy-Jean Michon, Christophe Josserand, and Thomas Séon. Jet dynamics post drop impact on a deep pool. Physical Review Fluids, 2(2):023601, 2017.

[20] Utkarsh Jain, Maziyar Jalaal, Detlef Lohse, and Devaraj van der Meer. Deep pool water-impacts of viscous oil droplets. Soft Matter, 15(23):4629–4638, 2019.

[21] Maziyar Jalaal, Dave Kemper, and Detlef Lohse. Viscoplastic water entry. Journal of Fluid Mechanics, 864:596–613, feb 2019.

[22] Hugh C. Pumphrey and Paul A. Elmore. The entrainment of bubbles by drop impacts. Journal of Fluid Mechanics, 220:539–567, 10 1990.

[23] Samuel Phillips, Anurag Agarwal, and Peter Jordan. The sound produced by a dripping tap is driven by resonant oscillations of an entrapped air bubble. Scientific Reports, 8(1), Jun 2018.

[24] Yuren Tian, Glynn Holt, and Robert E. Apfel. Investigation of liquid surface rheology of surfactant solutions by droplet shape oscillations: Experiments. Journal of colloid and interface science, 187:1–10, 1997.

[25] V. Thominet, C. Stenvot, and D. Langevin. Light scattering study of the viscoelasticity of soluble monolayers. Journal of colloid and Interface Science, 126(1):54, 1987.

[26] D. Vollhardt and G. Emrich. Coadsorption of sodium dodecyl sulfate and medium-chain alcohols at the air–water interface. Colloids and Surfaces A: Physicochemical and Engineering Aspects, 161:173–182, 2000.

[27] Ozgur E. Yildirim, Qi Xu, and Osman A. Basaran. Analysis of the drop weight method. Physics of Fluids, 17(6):062107–13, 06 2005.

[28] Ibrahim Sadek Khattab, Farzana Bandarkar, Mohammad Amin Abolghassemi Fakhree, and Abolghasem Jouyban. Density, viscosity, and surface tension of water+ ethanol mixtures from 293 to 323k. Korean Journal of Chemical Engineering, 29:812–817, 2012.

[29] Marcel Minnaert. Xvi. on musical air-bubbles and the sounds of running water. The London, Edinburgh, and Dublin Philosophical Magazine and Journal of Science, 16(104):235–248, 1933.

[30] F Minami and K Hasegawa. Cavity and jet formation after immiscible droplet impact into deep water pool. Physics of Fluids, 34(3):033315, 2022.

[31] Leng Jong Liow. Splash formation by spherical drops. Journal of Fluid Mechanics, 427:73–105, 2001.

[32] Bahni Ray, Gautam Biswas, and Ashutosh Sharma. Regimes during liquid drop impact on a liquid pool. Journal of Fluid Mechanics, 768:492–523, 2015.

[33] B.A. Noskov and D.O. Grigoriev. Capillary wave propagation on solutions of surfactants: a new method for kinetic studies. Progress in Colloid and Polymer Science, 97:1–5, 1994.

[34] J Lucassen and Robert S Hansen. Damping of waves on monolayer-covered surfaces: I. systems with negligible surface dilational viscosity. Journal of colloid and interface science, 22(1):32–44, 1966.

[35] J Lucassen and Robert S Hansen. Damping of waves on monolayer-covered surfaces: Ii. influence of bulk-to-surface diffusional interchange on ripple characteristics. Journal of Colloid and Interface Science, 23(3):319–328, 1967.

[36] Harishankar Manikantan and Todd M. Squires. Surfactant dynamics: hidden variables controlling fluid flows. Journal of Fluid Mechanics, 892, apr 2020.
[37] C. R. Constante-Amores, L. Kahouadji, A. Batchvarov, S. Shin, J. Chergui, D. Juric, and O. K. Matar. Dynamics of a surfactant-laden bubble bursting through an interface. Journal of Fluid Mechanics, 911(A57), 2021.
[38] M.A. Erinin, C. Liu, X. Liu, W. Mostert, L. Deike, and J.H. Duncan. The effects of surfactants on plunging breakers. Journal of Fluid Mechanics, 972, oct 2023.
[39] A. Prosperetti, L. A. Crum, and H. C. Pumphrey. The underwater noise of rain. Journal of Geophysical Research: Oceans, 94(C3):3255–3259, 1989.
[40] B. Néel, M. A. Erinin, and L. Deike. Role of contamination in optimal droplet production by collective bubble bursting. Geophysical Research Letters, 49(1), 2021.
[41] J. Pierre, M. Poujol, and T. Séon. Influence of surfactant concentration on drop production by bubble bursting. Physical Review Fluids, 7(073602), 2022.

Acknowledgements

The authors thank Fabien Gerbal for fruitful discussions and his expert assistance with image analyses, and Adrien Bussonière and Michaël Berhanu for fruitful discussions.